JGR Atmospheres

RESEARCH ARTICLE
10.1029/2022JD037881

The Role of Mineral Dust Aerosol Particles in Aviation Soot-Cirrus Interactions

B. Kärcher[1], C. Marcolli[2], and F. Mahrt[3]

[1]Institute for Atmospheric Physics, DLR Oberpfaffenhofen, Wessling, Germany, [2]Institute for Atmospheric and Climate Science, ETH Zürich, Zürich, Switzerland, [3]Laboratory of Environmental Chemistry, Paul Scherrer Institute, Villigen, Switzerland

Key Points:

- Mineral dust outcompetes contrail-processed aviation soot in aerosol-cirrus interactions
- Mineral dust reduces homogeneously nucleated ice crystal numbers more effectively than aviation soot
- Strong potential of pre-existing cirrus clouds to suppress new cloud ice formation

Correspondence to:

B. Kärcher,
bernd.kaercher@dlr.de

Citation:

Kärcher, B., Marcolli, C., & Mahrt, F. (2023). The role of mineral dust aerosol particles in aviation soot-cirrus interactions. *Journal of Geophysical Research: Atmospheres*, *128*, e2022JD037881. https://doi.org/10.1029/2022JD037881

Received 20 SEP 2022
Accepted 6 JAN 2023

Author Contributions:

Conceptualization: B. Kärcher
Formal analysis: B. Kärcher, C. Marcolli, F. Mahrt
Investigation: B. Kärcher, C. Marcolli, F. Mahrt
Methodology: B. Kärcher
Validation: B. Kärcher, C. Marcolli, F. Mahrt
Writing – original draft: B. Kärcher
Writing – review & editing: B. Kärcher, C. Marcolli, F. Mahrt

Abstract Predicting cirrus cloud properties with confidence requires a sound understanding of the relative roles of homogeneous and heterogeneous ice formation. This study explores the effect of mineral dust and contrail-processed aviation soot particles as ice-nucleating particles (INPs) competing with liquid solution droplets in cirrus formation. We study aerosol-cirrus interactions by accounting for atmospheric variability in updraft speeds and INP number concentrations. Our results confirm the dominant role of mineral dust in ice nucleation events in cirrus clouds. In addition, we show that pre-existing thin cirrus may suppress ice formation when updraft speeds are low. We find that homogeneous freezing of liquid solution droplets dominates clear-sky aerosol-cirrus interaction above a threshold updraft speed determined by total number concentrations and ice nucleation abilities of INPs. When mineral dust particles exceed number concentrations of 10 L^{-1}, they reduce homogeneously nucleated ice crystal numbers significantly and even prevent homogeneous freezing for frequently observed local updraft speeds between 10 and 20 cm s^{-1}. When both mineral dust and aviation soot particles coexist with solution droplets, dust typically prevents ice nucleation by aviation soot. Aviation soot exerts a notable impact on cirrus ice numbers only if updrafts are weak, large soot particles are present in number concentrations that are considerably higher than typically observed in emission measurements, and/or number concentrations of mineral dust and other INPs are low. Overall, our results elucidate the role of aviation soot-cirrus interactions in the presence of other INP types.

Plain Language Summary Understanding ice formation from atmospheric aerosol particles in cirrus clouds is important to correctly predict the impact of cirrus on climate. Here, we study for the first time on the process level cirrus ice formation from freezing of liquid solution droplets in competition with ice nucleation on mineral dust and aviation-produced soot particles. Our results show that in the majority of cloud-forming updrafts, mineral dust particles dominate cirrus formation over droplet freezing and that they outcompete aviation soot in producing cloud ice. Moreover, already existing cirrus clouds often prevent ice formation from these particle types altogether. Our results help evaluate cirrus parameterizations within global models and constrain model-based estimates of the global climate impact of aviation.

1. Introduction

Cirrus clouds are critical at modulating Earth's energy budget (Forster et al., 2021). These pure ice clouds can form by homogeneous freezing of ubiquitous liquid solution droplets. At cirrus conditions in the upper troposphere (UT), ice formation can be facilitated by ice-nucleating particles (INPs), a small fraction of the atmospheric aerosol population.

To correctly predict cirrus microphysical and optical properties, knowledge of the relative importance between ice nucleation induced by solution droplets and INPs (hereinafter referred to as "competing nucleation") is required. Especially when competing nucleation is involved, predictions of aerosol-cirrus interactions in global models are challenging, because the mechanisms of cirrus formation are not resolved on the computational grid of such models and therefore need to be parameterized. However, key elements of such parameterizations, including nucleation properties of different INP types and local cooling/heating rates generated by vertical wind speed fluctuations, are often implemented in models based on highly simplified schemes. Moreover, field observations of composition and abundance of INPs in the cirrus regime are sparse. As a consequence, global model results of aerosol-cirrus interactions remain associated with large uncertainties (Kreidenweis et al., 2019).

Measured ice nucleation spectra extend over a range of supersaturation values, consistent with experimental evidence for the vast majority of INP types. Whether heterogeneous ice nucleation occurs sharply around a fixed ice supersaturation or gradually across a range of values may affect the integrated water vapor loss during cirrus formation (see Figure 1 in: Kärcher (2022), hereinafter referred to as K22) and thus, homogeneously nucleated ice crystal number concentrations (ICNCs). Therefore, traditional parameterization schemes that employ a single threshold supersaturation to represent ice nucleation from INPs will have difficulties representing total ICNC changes due to competition between heterogeneous and homogeneous nucleation. This is especially important in the case of INPs that become ice-active only alongside homogeneous freezing. For this reason, we employ a novel cirrus parameterization that accounts for gradual heterogeneous ice formation (K22).

Mineral dust aerosol particles are known to be efficient INPs (DeMott et al., 2003). Recent global-scale measurements have increased our knowledge on number concentration and sizes of UT mineral dust particles (Froyd et al., 2022). Global climate model simulations indicate that dust emissions may lead to significant global radiative effects and thus have the potential to perturb climate (Kuebbeler et al., 2014). By contrast, the ability of aerosol particles emitted from combustion processes to nucleate ice is much less understood (Kanji et al., 2017). Combustion aerosols include a wide array of biomass burning and soot particles (Bond et al., 2013). Global climate model simulations indicate that soot particles can affect thin cirrus clouds, and may thereby cause a moderate negative radiative forcing (RF) (McGraw et al., 2020).

Aircraft emit copious soot particles directly in the UT (Anderson et al., 1999). When subsequently processed in contrails, the released soot particles (hereinafter referred to as "aviation soot") can modify cirrus microphysical properties (Kärcher et al., 2021) (hereinafter K21). Contrail processing refers to the formation and subsequent full sublimation of contrail ice crystals, each containing one emitted soot particle at their cores. This process generates compacted soot aggregates with enhanced ice nucleation activity (Mahrt et al., 2020). Although only a part of all soot particles emitted by aircraft undergoes contrail processing, cirrus clouds may frequently be affected by aviation soot INPs in the northern hemisphere (NH), where most aviation activity occurs.

Aviation soot-cirrus interactions rank among the most controversial processes *du jour* contributing to the climate impact of aviation (Lee et al., 2021). Global climate model simulations provide a wide range of associated RF values. The large spread of RF is mainly caused by the underlying parameterizations of the ice activity of aviation soot, which rely on disparate assumptions. For example, some climate models parameterize ice formation from aviation soot at ice supersaturation considerably lower than that needed for homogeneous freezing (Penner et al., 2018; Righi et al., 2021; Zhu et al., 2022), allowing aviation soot to readily contribute to the formation of cirrus clouds. The corresponding model simulations predict large RF values from aviation-soot cirrus interactions. By contrast, other climate model simulations that prescribe higher ice supersaturation thresholds for aviation soot to become ice active lead to small RF values (Gettelman & Chen, 2013; Pitari et al., 2015; Righi et al., 2021).

Due to the lack of conclusive evidence of aviation soot ice nucleation effects from *in-situ* observations, ice formation parameterizations used within these climate models are mostly specific to soot particles tested in laboratory experiments, which are larger than the vast majority of ambient aviation soot particles. To account for this systematic difference, we have developed the pore condensation and freezing (PCF) framework that allows to generally describe soot-induced ice nucleation based on the underlying particle morphology and other key particle properties (Marcolli et al., 2021). INPs described by PCF possess pores in which water can condense and freeze homogeneously. The soot PCF framework is not specific to an individual soot type tested in the laboratory, but describes a wide range of ice nucleation laboratory data well by accounting for the actual soot particle properties, in particular size and hydrophilicity, used in the respective measurement. Importantly, PCF replicates the strong size dependence of the ice supersaturation required for ice activation found in laboratory investigations.

The development of the PCF framework together with recent progress in quantifying ice nucleation abilities of atmospheric mineral dust particles (Brunner et al., 2021; Gao & Kanji, 2022b; Marcolli et al., 2021) and vertical wind speed variability (Kärcher & Podglajen, 2019; Podglajen et al., 2016; Schoeberl et al., 2017) motivates us to investigate competing nucleation involving solution droplets, mineral dust, and aviation soot particles. In view of the high ice supersaturation required by aviation soot particles to form ice crystals (K21), the question arises whether they are able to compete with more efficient INPs such as mineral dust, even if typically present in much higher amounts.

Table 1
Overview of Model Simulations Describing Cirrus Formation

Case	Features
Hom	Homogeneous freezing of supercooled liquid solution droplets
Pre	Hom + 10 L^{-1} pre-existing cirrus ice crystals (r_m = 30 µm)
Soot	Hom + 500 L^{-1} soot particles (D_m = 29.3 nm, σ = 1.72)
Dust	Hom + 28 L^{-1} dust particles
All	Hom + Soot + Dust

Note. Cases Hom and Pre assume pure homogeneous freezing without and with pre-existing ice crystals, respectively. Cases Soot and Dust refer to contrail-processed aircraft soot emissions and dust particles added as INPs to the liquid solution droplets, respectively. Moreover, r_m is the radius of monodisperse cirrus ice crystals and D_m and σ are the geometric mean mobility diameter and geometric standard deviation of log-normally distributed aviation soot particles taken from *in-situ* data. The dust particle size distribution is also taken from *in-situ* measurements, see Figure A1a. All cases are evaluated at an air temperature (pressure) 220 K (250 hPa) and updraft speeds representative of values measured at cirrus levels.

Here, we allow mineral dust and aviation soot particles to compete among each other as well as with solution droplets in ice nucleation events. Moreover, we account for variability in updraft speeds as well as in total soot and dust particle number concentrations to capture atmospheric complexity. Thereby, we investigate aviation soot-cirrus interactions under increasingly realistic atmospheric conditions, which allow to place constraints on results of global model simulations. As new ice formation may also take place within pre-existing cirrus clouds (X. Shi et al., 2015), we also address the potential of ice crystals either stemming from pre-existing thin cirrus or from settling from higher altitude cirrus (fall streaks) into air parcels to modify or prevent new ice formation.

The paper is organized as follows. After presenting the model approach and microphysical properties of the two INP types involved in our study—mineral dust and contrail-processed aviation soot—in Section 2, we discuss fundamental insights into aerosol-cirrus interactions and explore the role of atmospheric variability in Section 3. Section 4 clarifies recent laboratory studies of INP activation and discusses our results in the light of climate model studies that suggest a substantial role of aviation soot in aerosol-cirrus interactions. Section 5 concludes our study by summarizing its main findings.

2. Methods

2.1. Modeling Approach and Set-Up of Simulation Cases

The K22 parameterization employed in this study is able to predict total nucleated ICNCs along with the associated peak ice supersaturation attained in cirrus ice nucleation events. It replicates results for these variables from more detailed numerical simulations well and has been validated with simulations of mineral dust and aviation soot particles acting as INPs.

To focus on effects of aviation soot emissions on cirrus formation, we choose meteorological conditions representative for midlatitude regions, for example, typical values of UT air temperature (T = 220 K) and pressure (p = 250 hPa). We first drive the parameterization with constant updraft speeds to gain basic insight in how competing nucleation influences key parameters such as peak ice supersaturation and total ICNCs in cirrus clouds. In a second set of simulations, we use variable updraft speeds sampled from probability distributions to statistically analyze key properties of aviation soot-cirrus interactions.

Table 1 lists the different simulation cases discussed in this work. We note that cases Hom and Soot are equivalent to cases Base and Background in K21. While the Background case in K21 was based on large soot particles, here we vary soot particle sizes, using average log-normal size distribution parameters in case Soot as a default. The selected radius r_m of monodisperse cirrus ice crystals in case Pre is close to typical effective radii observed in cirrus (Hong & Liu, 2015). A cirrus ICNC of 10 L^{-1} may be viewed as typical for optically thin cirrus or fall streaks. Case Pre is difficult to capture in low-resolution models, which do not resolve individual clouds. Associated experimental evidence is also difficult to infer from *in-situ* observations, for example, due to the presence of INPs.

Ice nucleation parameterizations implemented in global models should be carefully validated with respect to dynamical forcing, aerosol particle properties, and competing nucleation. In this context, we reiterate that a change in mean updraft speed of 10% leads to a change in homogeneously nucleated ICNC of 15% (K22), which already supersedes the average aviation soot effect. For the purpose of statistical analyses, we introduce variability in updraft speeds, w. This is achieved by random sampling from exponential distributions with standard deviations σ_w = 5–25 cm s^{-1}, or corresponding mean values, $\sigma_w/\sqrt{2}$. Such distributions are derived from observed Lagrangian time series of vertical wind speed fluctuations that result from mesoscale gravity waves (Podglajen et al., 2016). The above range of standard deviations encompasses typical mean updraft speeds measured at cirrus levels across all latitudes. It represents the dynamical forcing of *in-situ* cirrus formation away from distinct gravity wave sources such as mountains, fronts, or convection (Kärcher & Podglajen, 2019). We note that wave

forcing is transient and may exhibit marked local variations in σ_w (Jensen et al., 2013). To distinguish the three different σ_w-cases, we refer to the updraft regimes as weak (5 cm s^{-1}), average (15 cm s^{-1}), and strong (25 cm s^{-1}). Generally, INP effects on cirrus clouds are small in the presence of vigorous updrafts (>50–100 cm s^{-1}) favoring homogeneous freezing.

In all simulation cases, homogeneous freezing takes place on monodisperse liquid solution droplets that are characterized by a total number concentration of 500 cm^{-3} and a mean wet radius of 0.25 μm (Kärcher, DeMott et al., 2022). No sensitivity simulations were performed here, as the susceptibility of homogeneously nucleated ICNCs to liquid solution droplet number concentration and size is weak (Hoyle et al., 2005; Kärcher & Lohmann, 2002; Kay & Wood, 2008). Specifically, parcel simulations typically show that changes in solution droplet size distributions parameters (total number concentration, mean size, size spread) lead to only minor (<30%) changes in homogeneously nucleated ICNCs.

2.2. Microphysical Properties and Ice Activities of INP Types

A value of $n_s = 500$ L^{-1} for the total number concentration of aviation soot particles, approximately represents background (large-scale) conditions in the UT within or nearby busy air traffic corridors (K21). To include variability in our statistical analyses, we prescribe a normal distribution around this value with a standard deviation of 150 L^{-1} to cover the spread of values reported in a compilation of contrail ICNC data (Schumann et al., 2017). The geometric mean mobility diameter (29.3 nm) and geometric standard deviation (1.72) of the log-normally distributed aviation soot particle sizes are average values derived from airborne measurements of fresh aircraft emissions (Moore et al., 2017). As ice nucleation on aviation soot is strongly particle size-dependent, we distinguish between lower-limit (case Soot-S: 22.8 nm, 1.65) and upper-limit values (Soot-L: 35.7 nm, 1.8) from the same study. Case Soot-L maximizes the fraction of large soot particles (0.9% have mobility diameters >200 nm) across the number-based particle size distributions (PSDs) discussed in K21 that included bimodal distributions.

The ice activity of bare (uncoated) aviation soot is based on the soot PCF framework (Marcolli et al., 2021), employed with parameters that are representative for aviation soot particles, as described in K21. The highest ice-active aviation soot particle fractions are reached at high ice supersaturation, s, alongside homogeneous freezing ($s \approx 0.5$), depending on the assumed soot PSD (K21). Using the soot PCF parameterization is consistent with other studies that used PCF to predict ice formation on porous particles (Jantsch & Koop, 2021).

For mineral dust particles, we make use of data from *in-situ* measurements. Specifically, the size distribution data used here are campaign averages over the NH UT outside of dust-enhanced plumes reported by Froyd et al. (2022). While many of the samples contained only few dust particles (<1–10 L^{-1}), a total particle number concentration $n_d = 28$ L^{-1} is representative for conditions unaffected by rapid lofting of dust from the lower troposphere. Therefore, we distribute dust particle number concentrations normally around a mean value of 28 L^{-1} with a standard deviation of 12 L^{-1}. With regard to the ice activity of bare mineral dust particles, we combine the PSD with an ice-active site density parameterization for desert dust (Ullrich et al., 2017), as described in Appendix A. This causes dust INP populations to fully activate into ice crystals just above $s = 0.4$.

Pre-activation occurs when a microscopic ice phase from an initial ice nucleation event is retained in aggregates and causes the formation of macroscopic ice crystals in a subsequent cloud cycle. This process is negligible compared to PCF in forming ice on soot particles at cirrus levels (as discussed in K21) and thus is not considered here.

In cirrus models, a deposition coefficient, α, is frequently used to quantify the uptake of water vapor molecules on ice crystal surfaces. Values of α increase with increasing ice supersaturation (Lamb & Verlinde, 2011). The depositional (diffusional) ice crystal growth law contains a kinetic correction factor to take surface-related, molecular-level processes into account (Zhang & Harrington, 2014). Deposition coefficients for spherical ice crystals denote averages over values suitable for individual crystal facets. Besides growing by facets, especially small ice crystals with dimensions of several tens of micrometers as well as polycrystals that are frequently observed in cirrus, grow by dislocations (Harrington & Pokrifka, 2021). To date, the complexity of processes involved in deposition growth and the multitude of observed ice crystal habits prevents modeling the entity of cirrus ice crystal growth modes in detail.

In the parameterization employed here, we model water vapor uptake on spherical ice crystals with a constant deposition coefficient, corresponding to values during cirrus formation where ice crystals nucleate and grow

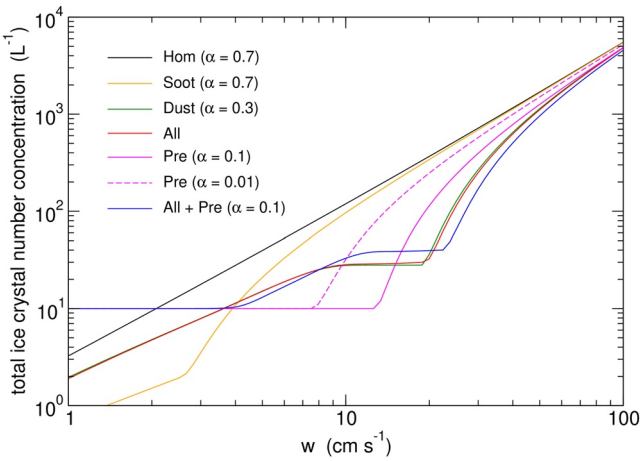

Figure 1. Ice crystal formation in clear sky and within pre-existing cirrus for $T = 220$ K and $p = 250$ hPa. Shown are total nucleated ICNCs versus updraft speed in the mesoscale range. Ice crystals nucleating from aviation soot particles (orange), dust particles (green), or from both types of INP together (red). Results from pure homogeneous freezing of liquid solution droplets without (black) and with (magenta) pre-existing ice crystals (included in the total ICNC) are shown for comparison. The dashed magenta curve is a sensitivity study with a tenfold reduced deposition coefficient for growth ($\alpha = 0.01$) of pre-existing cloud ice. The blue curve contains all types of INPs and pre-existing ice. Details of the simulation cases and results are listed in Tables 1 and 2, respectively.

from either mineral dust ($\alpha = 0.3$) or aviation soot INPs ($\alpha = 0.7$). These values have been shown by K22 to replicate results from numerical simulations employing supersaturation-dependent deposition coefficients. The value of the deposition coefficient for pre-existing ice crystals likely varies within and among cirrus clouds and with cloud age and is therefore less well constrained. As water vapor uptake does not change much when using values $\alpha = 0.1$–1 (K22, their Figure A1), we use $\alpha = 0.1$ in case Pre, since already existing cloud ice crystals are larger than those freshly nucleated and are thus characterized by a reduced uptake efficiency (Lamb & Verlinde, 2011). To model a situation with significantly reduced uptake, we also perform a sensitivity simulation with $\alpha = 0.01$ in case Pre.

3. Results

Fundamental insights into the role of mineral dust aerosol particles in modulating aviation soot-cirrus interactions are obtained through simulations with fixed values for w, n_s, and n_d (Section 3.1), followed by a statistical analysis of INP-cirrus interactions accounting for atmospheric variability in these parameters (Section 3.2).

3.1. Simulations With Constant Updrafts and INP Numbers

Figure 1 presents the total ICNC as a function of w. INPs are represented by soot ($n_s = 500$ L^{-1}) and dust ($n_d = 28$ L^{-1}) and the sum of both (All). Mineral dust particles and pre-existing ice crystals (10 L^{-1}) affect the nucleated ICNCs in the range of typically observed, wave-driven updraft speeds of 10–20 cm s^{-1}, corresponding to dry adiabatic cooling/heating rates in the range of approximately 4–8 K hr^{-1}. By contrast, aviation soot particles affect nucleated ICNCs mainly at updraft speeds smaller than 10 cm s^{-1}.

In the case of pure homogeneous freezing (Hom), ICNCs achieve values exceeding 100 L^{-1} for updraft speeds greater than about 10 cm s^{-1}. Within cirrus (case Pre with $\alpha = 0.1$ or $\alpha = 0.01$), water vapor consumption due to deposition growth of pre-existing cloud ice crystals suppresses homogeneous freezing below about 7.5–12.5 cm s^{-1}, depending on α. The impact of pre-existing cloud ice decreases only slowly with increasing w, approaching ICNCs from pure homogeneous freezing only above about 100 cm s^{-1}, that is, in vigorous updrafts generated by lee or convectively generated waves. The effect of pre-existing cloud ice on homogeneous freezing starts to diminish for low water vapor uptake efficiencies, as shown in case Pre using $\alpha = 0.01$. At this point, we recall that in cirrus clouds depending on ice supersaturation and ice crystal habits, α may be subject to large variability. We add that total cirrus ICNC is also highly variable and may in many cases be significantly larger than 10 L^{-1} (Krämer et al., 2021), diminishing the importance of INP effects and preventing homogeneous freezing until updraft speeds are sufficiently large for a given value of α.

In the simulation case Soot (dust), ICNCs increase with w up to about 3 (20) cm s^{-1}, because the associated increase in peak s-values reached during cloud formation enhances the fraction of particles that can act as INPs. At this point, ICNCs reach values of 2 L^{-1} (soot, partial activation) and 28 L^{-1} (dust, full activation). This difference in ICNCs reflects the fact that dust nucleates ice much more effectively than aviation soot, despite the latter particles are far more abundant. The plateau in case Dust marks the region where deposition growth of INP-derived ice crystals completely suppresses homogeneous ice nucleation by limiting the supersaturation increase with increasing w. In sufficiently strong updrafts, the consumption of water vapor by INP-derived ice crystals no longer prevents homogeneous freezing, leading to a pronounced increase in ICNC as w increases above 20 cm s^{-1}. Total ICNCs in cases Soot and Dust stay below the values found in case Hom when comparing the same updrafts. No plateau occurs in case Soot, because the aviation soot particles nucleate ice in relevant number concentrations only alongside homogeneous freezing (K21).

As mineral dust is a much more potent INP type than aviation soot, allowing both types to form ice simultaneously and compete for the available water vapor (case all) produces ICNCs that differ only marginally from those

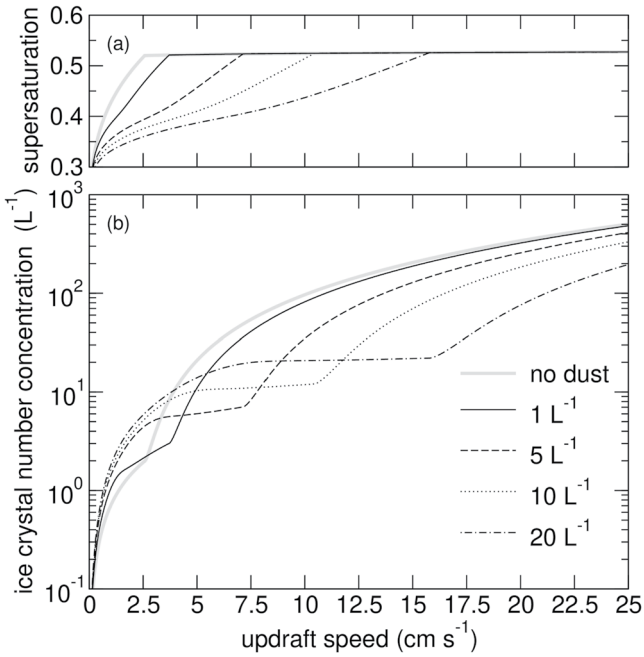

Figure 2. Aviation soot-cirrus interactions in the presence of dust. Peak ice supersaturation attained in the ice nucleation events (a) and total nucleated ICNC (b) versus updraft speed for selected total dust particle number concentrations. In all simulation cases, the total aviation soot particle number concentration is 500 L^{-1}. The gray curve marks the pure aviation soot case.

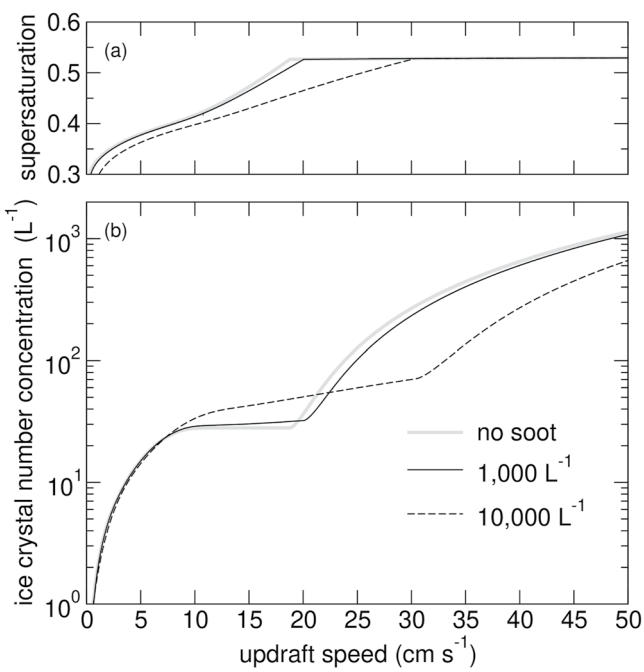

Figure 3. Dust-cirrus interactions in the presence of aviation soot. Peak ice supersaturation attained in the nucleation events (a) and total nucleated ICNC (b) versus updraft speed for selected total aviation soot particle number concentrations. In all simulation cases, the total dust particle number concentration is 28 L^{-1}. The gray curve marks the pure dust case.

found in case Dust. We see the situation emerging where already a few dust particles can outcompete aviation soot in aerosol-cirrus interactions. Adding pre-existing ice crystals to case All is able to shift the onset of homogeneous freezing by about 10% (2 cm s^{-1}), because they consume additional water vapor during growth.

In Figure 2, we illustrate the impact of dust in aviation soot-cirrus interactions, focusing on case All in the range of updraft speeds up to 25 cm s^{-1}, where the effect of dust particles is most pronounced (Figure 1). To better understand the peak s-values attained during ice nucleation events, $\hat{s}$ (Figure 2a), we note that homogeneous freezing sets in above a dust-dependent threshold updraft speed, characterized by $s > 0.5$ and $\hat{s}$-values that stay almost constant, because an additional dependence of $\hat{s}$ on w is weak. Comparison with the no dust case reveals that even 1 L^{-1} dust particles are capable of modifying the activation of aviation soot particles and shifting the onset of homogeneous freezing to a slightly higher updraft speed (from 2.5 cm s^{-1} to 3.7 cm s^{-1}, Figure 2b). Increasing n_d to 5 L^{-1} extends the dominating effect of dust on ICNC to 7.5 cm s^{-1} (deflection in the dashed curve in Figure 2b). For $n_d > 10$ L^{-1}, the presence of aviation soot becomes irrelevant and dust dominates the cirrus formation process across the range of typically observed mean updraft speeds (10–20 cm s^{-1}).

In a complementary way, Figure 3 shows the impact of aviation soot in dust-cirrus interactions. Comparison with Figure 2 reveals the limited effect of aviation soot compared to dust. The addition of 1,000 L^{-1} aviation soot particles does not significantly modify the dust impact. Only when present in very high number concentrations do aviation soot particles exert a notable impact on nucleated ICNCs. We note that for example, 10,000 L^{-1}, represents a residual soot particle number concentration after dissipation of short-lived contrails (age about 1, 000 s) (K21).

We conclude that cirrus cloud ice may form exclusively on aviation soot particles only at low updraft speeds (several cm s^{-1}) and in regions with low dust particle number concentrations (<5 L^{-1}). The resulting cirrus contain only few ice crystals per liter of air, making them optically very thin clouds. In stronger updrafts, homogeneous freezing sets in, leading to a nucleation burst with the resulting ICNC modulated by the number of available dust and aviation soot particles. These findings are entirely consistent with previous results of cloud simulations that did not consider mineral dust (K21).

3.2. Role of Atmospheric Variability

To represent atmospheric variability, we evaluate the ice nucleation parameterization with aviation soot and dust as INPs for 2,500 different combinations of w-, n_s- and n_d-values that were sampled randomly from their respective distributions (Section 2). This statistical approach captures the variability of key factors affecting aerosol-cirrus interactions, ultimately allowing to more realistically assess the impact of aviation soot on cirrus cloud microphysical and radiative properties. The results are shown in Figure 4 and quantitative information of the key variables is listed in Table 2.

Each panel in Figure 4 presents two data categories. The category termed "pure" (circles without black outlines) contains only INP-induced ice nucleation events. Category "comp" (circles with black outlines) includes all data in which both, homogeneous and INP-induced nucleation occurred. The wide range of simulated ICNCs, from almost 10,000 L^{-1} to below 0.1 L^{-1}, is

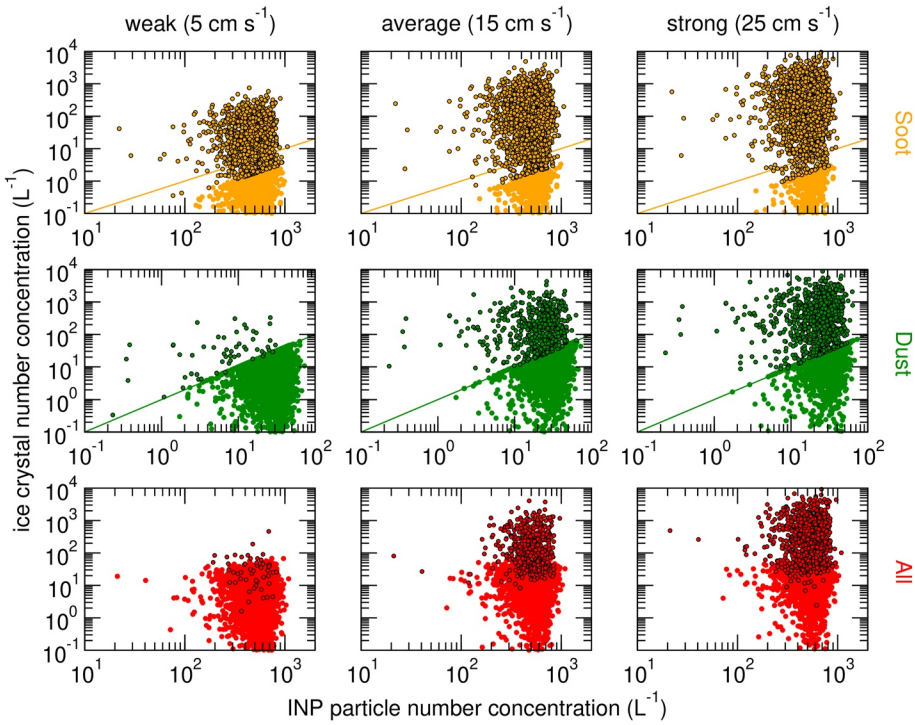

Figure 4. Ensemble simulations of competing nucleation where both aviation soot and dust can act as INPs. Total nucleated ICNC versus INP particle number concentration for three wave-driven forcing regimes (columns), corresponding to standard deviations of updraft speeds, σ_w, as indicated. Cases (rows) as defined in Table 1. For each simulation, filled circles mark the subset of data ("pure") in which only INPs formed ice ("pure"), and those with black outlines mark data affected by competing homogeneous and INP-induced nucleation ("comp"). Lines indicate 1% ice activity in case Soot and 100% ice activity in case Dust.

mainly caused by the imposed variability in updraft speeds. This broad distribution of nucleated ICNCs points to homogeneous freezing as the key background process modulated by the presence of INPs, whereby the strongest updrafts trigger rare yet massive homogeneous freezing events (ICNC >1, 000 L^{-1}).

Regardless of the INP type, the number of "pure" data points decreases and those in "comp" increase when going from weak to strong dynamical forcing (see also Table 2). This happens because deposition growth of INP-derived ice crystals is less likely to quench (deplete) the larger ice supersaturation reached in stronger updrafts.

In each forcing regime, the number of "pure" data points is larger in case Dust than in case Soot, since dust is a better INP capable of preventing homogeneous freezing more effectively under various atmospheric conditions. As mentioned before, aviation soot nucleates ice in considerable numbers only close to the homogeneous freezing supersaturation threshold. Therefore, its ability to quench the supersaturation before homogeneous freezing levels are reached is limited. Generally, "comp" data points are correlated with high updraft speeds. The fewest data points in this category are thus seen for weak forcing in case all, where the quenching effects of both aviation soot and dust add up. For the case Soot and strong forcing, we find the most "comp" data points (Table 2).

Regardless of the updraft regime, only about 0.3% of aviation soot particles become ice-active across a typical PSD (orange curve in Figure A2c). Thus all "pure" data points in case Soot stay well below the upper-limit 1%-ice activity line, as suggested by K21. In case Soot-S, the maximally activated fraction decreases further to 0.08% while in Soot-L it increases to almost 1%, see magenta and cyan curves in Figure A2c, respectively. Accordingly, the relative importance of "pure" ice nucleation events increases with increasing soot particle sizes (Table 2). By contrast, all dust particles can be activated, as the "pure" data points extend to the 100%-ice activity lines in case Dust in each forcing regime. Adding both types of INPs together (all) blurs the distinction between "pure" and "comp" data subsets that is seen for the individual INP types.

Closer inspection of Table 2 shows that dust particles play an important role in the total data set (case All), as they limit the average peak supersaturation to values between 0.36 and 0.44, indicative of ample "pure" events.

Table 2
Ensemble Statistics Given for Distinct Wave-Driven Forcing Regimes (Defined by Standard Deviations of Exponentially Distributed Updraft Speeds, σ_w) for the Baseline Simulations Soot, Dust, All, and the Sensitivity Studies Soot-S and Soot-L

Case		Mean (median) ICNC [L^{-1}]			$\hat{s}$			f [%]		
σ_w ($cm\,s^{-1}$)	Category	5	15	25	5	15	25	5	15	25
Hom	Total	34 (14)	200 (74)	464 (164)	0.520	0.523	0.524	100	100	100
Soot-S	Pure	0.23 (0.20)	0.23 (0.20)	0.23 (0.20)	0.443	0.441	0.443	21	8	5
	Comp	39 (18)	212 (86)	485 (185)	0.521	0.524	0.525	79	92	95
	Total	30 (9)	193 (66)	457 (157)	0.487	0.512	0.517	100	100	100
Soot	Pure	0.88 (0.73)	0.94 (0.81)	0.99 (0.90)	0.425	0.429	0.433	49	22	14
	Comp	45 (22)	226 (92)	516 (215)	0.522	0.524	0.526	51	78	86
	Total	23 (2)	175 (49)	441 (141)	0.458	0.499	0.509	100	100	100
Soot-L	Pure	2.2 (1.7)	2.6 (2.3)	2.8 (2.3)	0.408	0.421	0.427	75	39	27
	Comp	54 (28)	252 (113)	558 (234)	0.524	0.525	0.526	25	61	73
	Total	14 (2.5)	155 (24)	407 (103)	0.422	0.480	0.497	100	100	100
Dust	Pure	9 (6)	17 (15)	19 (18)	0.359	0.390	0.400	97	79	62
	Comp	35 (21)	305 (151)	650 (272)	0.523	0.527	0.528	3	21	38
	Total	10 (6)	78 (20)	260 (30)	0.352	0.415	0.446	100	100	100
All	Pure	9 (6)	17 (15)	19 (19)	0.358	0.390	0.399	98	81	63
	Comp	39 (22)	315 (164)	660 (275)	0.524	0.527	0.528	2	19	37
	Total	10 (6)	75 (20)	253 (30)	0.349	0.412	0.444	100	100	100

Note. Category "Pure" contains the subset of data in which only INP-induced ice nucleation occurred, in "Comp" both homogeneous and INP-induced nucleation occurred, and "total" includes both subsets. For comparison with categories "Total" in each case, we list results for homogeneous freezing (Hom). Listed are mean (median) nucleated ICNCs, Average peak ice supersaturation reached during the nucleation events, $\hat{s}$, and fractions of data points, f, are computed for each category (N_{pure}/N_{total} and N_{comp}/N_{total}, respectively, with the number of data points, N). A small number of data points with $w < 1$ mm s^{-1}, leading to insignificant ICNCs, were not included in the analysis.

By contrast, aviation soot will mostly contribute to cirrus formation at considerably higher s-values alongside homogeneous freezing, except for large particles (Soot-L) and weak forcing. As already suggested by Figure 1, cases Dust and All are very similar, because dust dominates ice nucleation.

While dust exerts a major influence on cirrus formation across all forcing conditions, the ICNC is limited to dust numbers (category "pure") or to maximally activated aviation soot numbers (a few per liter of air) in weak updrafts. In stronger updrafts, this limitation shifts to higher INP number concentrations, as more particles are needed to prevent homogeneous freezing. Although INPs are not able to prevent homogeneous freezing in stronger updrafts, they nevertheless reduce the number of homogeneously nucleated ice crystals. This happens to occur in the majority of all the cases investigated and may be quantified by comparing the highest possible mean ICNC from case Hom with any of the "total" ICNC data in the simulations Dust, Soot, and All. For instance, for an average forcing, this reduction amounts to $(200 - 175 =)25\ L^{-1}$ (12.5%) in case Soot and to $(200 - 78 =)122\ L^{-1}$ (61%) in case Dust in the ensemble data. We note that case Hom cannot be directly compared to "comp" data points. By design, the latter category lacks low ICNC data points from updrafts so weak that homogeneous freezing does not occur, hence, mean updrafts in category "comp" are higher than in the corresponding Hom cases, biasing "comp" mean and median ICNCs toward higher values.

4. Discussion

We critically evaluate the ice-active fractions for dust and aviation soot used in our model calculations (Section 4.1) and discuss implications for the climate impact of aviation soot-cirrus interactions, the evaluation of their effect predicted by climate models, and the prospect to isolate them in field measurements (Section 4.2).

4.1. Ice Activities of Mineral Dust and Aviation Soot

The relative importance of dust and soot INPs stems from the ice activity of mineral dust particles calculated with the parameterization of Ullrich et al. (2017) and the aviation soot PCF parameterization of Marcolli et al. (2021).

Mineral dust particles are known to be efficient atmospheric INPs (Kanji et al., 2017). Despite numerous desert and arid surface sources, only a small fraction of emitted dust particles reach the UT (Froyd et al., 2022) and many of them experience processing in supercooled liquid and mixed-phase clouds prior to reaching the UT (Wiacek & Peter, 2009). The mineral dust abundance is regionally and seasonally variable. Ullrich et al. (2017) formulated the ice-active fraction of desert dust at cirrus conditions using an ice nucleation active surface site density parameterization that is a function of T and s. It is based on laboratory measurements performed with desert dust samples collected from four different locations around the globe, covering temperatures down to 206 K. Ice nucleation sites in this parameterization may be understood as deposition nucleation sites or, more likely in view of recent findings, as pores suitable for PCF. Formulated as an active site density per surface area, the parameterization predicts increasing ice activity with increasing particle size irrespective of dust properties such as porosity or mineralogical composition. Moreover, it predicts increasing ice activity with decreasing temperature and increasing supersaturation.

For the present study, we apply this parameterization to a PSD derived from recent UT aircraft measurements outside of dust plumes (Froyd et al., 2022). Covering the size range 0.2–5 μm, these measurements feature a PSD that is dominated by the submicron fraction around 300 nm, as is expected for mineral dust after long-range transport in the atmosphere (see Appendix A). We derive for $T = 220$ K an ice-active fraction of 0.2 at $s = 0.35$ and full activation at $s = 0.425$, that is, before solution droplets freeze homogeneously.

Mineral dust particles with diameters smaller than 2 μm mainly consist of minerals such as illite, kaolinite, and montmorillonite (clay fraction). These are soft minerals that easily break up into smaller particles (Murray et al., 2012). By contrast, feldspars and quartz, which often dominate airborne mineral dust masses close to sources, are hard minerals that belong together with calcite to the coarser silt and sand fractions. Therefore, we expect the UT submicron particles to mainly consist of clay minerals. Clay particles have an inherently high porosity, as they consist of thin sheets randomly stacked to platelets (Mukherjee, 2013). The irregular stacking results in ragged edges that frame wedge-shaped pores (Marcolli, 2014, 2020; Wang et al., 2016). Clay minerals proved to be highly ice-active in continuous-flow diffusion chamber (CFDC) experiments at cirrus temperatures (218–223 K), realizing activated fractions of 0.2 at $s = 0.1$–0.2 when testing size-selected kaolinite, illite, and montmorillonite particles with diameters of 200, 400, and 800 nm (David et al., 2019; Welti et al., 2009). These studies also revealed that clay mineral particles with diameters of 100 nm proved to be ice-active, yet, with clearly lower activated fractions in most cases. Laboratory experiments reporting the total fraction of the entire (test) particle population to become active prior to homogeneous freezing are scarce. David et al. (2019) observed full activation for 400 nm illite particles around $s = 0.5$ at $T = 223$ K in their CFDC experiments. Möhler et al. (2008) report almost full activation at $s = 0.05$–0.2 for illite, and even at $s = 0.05$–0.15 for Arizona test dust (ATD) in their expansion chamber experiments. ATD is a commercial milled dust sample consisting of clay minerals, quartz, and feldspars (Kaufmann et al., 2016).

In conclusion, the assumption of full ice activation of dust particles before homogeneous freezing starts is realistic. Yet, we point out that based on the available laboratory data, the Ullrich et al. (2017) parameterization may underestimate the ice-active dust fraction at low supersaturation. Such an underestimation would further count toward our finding that cirrus formation is dominated by mineral dust relative to aviation soot.

Number concentrations of aviation soot particles are usually high within and close to air traffic corridors, and might therefore affect cirrus formation despite being poor INPs (Kärcher et al., 2007). Soot aggregate morphology and the presence of cavities have been found key for its ice activity (Bi et al., 2017; Mahrt et al., 2018; Nichman et al., 2019; Zhang et al., 2020). Moreover, cloud processing has been found to lead to a compaction of soot aggregates (Bhandari et al., 2019; China et al., 2015) and compacted soot aggregates have been reported to have enhanced ice nucleation activity (Gao et al., 2022; Mahrt et al., 2020). This enhancement in ice nucleation activity can consistently be described by an associated increase in the occurrence of suitable mesopores acting as ice nucleation sites (Marcolli et al., 2021). Compaction is a mechanical process that can be well replicated and studied in laboratory settings. Depending on the assumed soot PSD (K21), up to 0.9% of all soot particles become ice-active during cooling in the soot PCF parameterization before homogeneous freezing of solution droplets

sets in (Figure A2c). The parameterization predicting these low ice-active fractions represents ice activity of aviation soot particles in terms of soot aggregate size, primary particle diameter, and hydrophobicity (Marcolli et al., 2021), as found in laboratory experiments with aviation soot surrogates. The low activated fractions reached at the onset of homogeneous freezing for all soot cases examined in Section 3 (Soot-S, Soot, Soot-L) can be traced back to the small aggregate sizes typical for aviation soot formed in jet engine combustors (K21).

Both, the mineral dust and soot ice activity parameterizations are based on measurements of uncoated particles. In the atmosphere, aerosol particles often become internally mixed with secondary material such as organics, sulfate, nitrate, and ammonium during transport (Froyd et al., 2019; Sullivan et al., 2007; Z. Shi et al., 2008). It is often assumed that this material deposits as a uniform coating covering the particle surface, even though condensation in pores or adsorption as patches on the surface is more likely. Laboratory studies have shown that coating of particles may reduce or inhibit their ice nucleation at cirrus temperatures, depending on the composition and thickness of the coating (Cziczo et al., 2009; Gao & Kanji, 2022b; Koehler et al., 2010; Möhler et al., 2008; Primm et al., 2017). When particles form ice via PCF, coatings should hamper ice nucleation when they block pores, as measured in the case of soot (Gao & Kanji, 2022a). Yet, a thin coating may even facilitate water condensation and ice growth in case of wider pores or when the adsorbed material renders the particle surface more hydrophilic (Marcolli, 2017; Marcolli et al., 2021).

In a recent study, Gao and Kanji (2022b) investigated the simultaneous impact of cloud processing and thermal denuding on the ice nucleation activity of two soot types with low and high organic carbon content, respectively. These experiments allowed to assess the relative importance of particle porosity and wettability from changes in morphology and organic carbon content on the ice nucleation of the soot particles. Their results suggest that while denuding, an associated loss of volatile material leads to an increased soot particle porosity and wettability and thus ice nucleation ability, enhancement of particle porosity from cloud processing (i.e., physical compaction) dominates the changes in ice nucleation activity of these two soot samples.

As another example, Primm et al. (2017) found a similar ice nucleation onset supersaturation for illite mixed with organic acids as for pure illite, when the mixture was dominated by illite (mixing ratios >1) in cold stage experiments at 220 K. They observed an inhibiting effect of the organic coating once it had reached equivalent monolayer coverage on the illite particles. Möhler et al. (2008) found a reduction of ice activity for ATD particles with 17 wt.-% coating of secondary organic material (SOM) and a complete inhibition for illite particles with 41 wt.-% SOM coating. Froyd et al. (2019) estimate typical organic coatings that add 5–10% to the mass of ambient dust particles. Such coatings lead to less than a monolayer-equivalent surface coverage, which is expected to have only a minor impact on their ability to form ice via PCF. Coatings on soot exert similar effects on PCF as coatings on mineral dust and have been discussed in detail in Marcolli et al. (2021).

In summary, condensation of secondary material affects the ice activity of dust and soot similarly, and can generally be expected to shift the prevailing cloud forming mechanism from INP-induced to homogeneous ice nucleation.

4.2. Aviation-Soot Cirrus Interactions

It is difficult to track the causes of large radiative effects from aviation-soot cirrus interactions predicted by some global models, because of many interdependent model components contributing to such effects. Confounding factors include the underlying ice nucleation model, the simulated INP number concentrations, the updraft speeds employed to drive the nucleation paramaterization, and how perturbed cloud microphysical properties translate into radiative flux changes, hence RF.

For example, the global climate model parameterization used in Penner et al. (2018) and Zhu et al. (2022) specify $s = 0.35$ as a single ice supersaturation threshold for aviation soot particles with fewer than 3 monolayers of sulfate coating to nucleate ice at cirrus temperatures. This causes aviation soot to be more ice-active than mineral dust. Similarly, Righi et al. (2021) ascribe a wide range of ice nucleation efficiencies (including low activity thresholds $s \leq 0.4$ and high maximum activated fractions >1%) to aviation soot. While such choices capture the ice nucleation activities observed in some laboratory experiments for the most ice-active soot types and for large soot particle aggregates of 400 nm diameter, they do considerably overestimate the ice nucleation activities of aircraft-emitted soot particles, which are mainly composed of smaller aggregates (Moore et al., 2017). For instance, Gao et al. (2022) recently showed that 60 nm diameter soot particles, more representative for real-world aircraft soot emissions, do not contribute to ice formation at temperatures between 218 and 233 K.

As a result, the average reduction of homogeneously nucleated ICNCs, which is the basis for the large radiative effect ascribed to aviation soot reductions in Zhu et al. (2022), will be overestimated. We recall that for a typical mean updraft speed value σ_w = 15 cm s^{-1}, the reduction in total ICNCs in case Soot relative to case Hom amounts only to 3.5–22.5%, depending on the assumed PSD (Table 2). Clearly, it is important that the improved process understanding presented here regarding dust-aviation soot-cirrus interactions is incorporated into global model parameterizations. Although mineral dust INPs are included in global climate models (Righi et al., 2021; Zhu et al., 2022), predicted aviation soot effects are not discussed in relation to simulated dust and soot particle number concentrations.

To better constrain the ice nucleation activity of aviation soot, the particle's mixing state and size distribution (including total number concentration) must be known *after* processing in contrails (K21). ICNC data based on satellite or airborne observations alone are unlikely to fully constrain aviation soot-cirrus interactions. The largest uncertainties in measuring cirrus ICNCs occur in detecting small ice crystals with maximum dimensions up to some 10 μm just after ice nucleation events. While to date total ICNCs can generally be detected *in-situ* within a factor of 2 uncertainty (Baumgardner et al., 2017), reductions in homogeneously nucleated ICNCs of 12.5% (case Soot) and 61% (case Dust) for average forcing (Section 3.2) may escape detection, even if the transient nucleation stage is captured in *in-situ* measurements. In the case of aviation soot, the biggest effects should occur in regions with weak forcing conditions where at the same time high soot particle number concentrations coincide with low dust numbers. This means that vertical wind speed, its variability, and INP number concentration and composition should be measured alongside nucleated ICNCs to allow for a more holistic data analysis and to better constrain model simulations.

While a parcel model framework as used here simulates the ice formation stage, simulating the life cycle and integrated radiative effect of cirrus clouds with confidence requires the use of cloud- or cloud system-resolving models. We took a first step in this direction by applying a one-dimensional cirrus model that includes ice crystal sedimentation to simulate ice crystal size distributions more realistically (K21). The results of this study suggested that changes in cirrus ICNCs due to contrail-processed aviation soot may not significantly alter column optical depth over the first hour past formation.

5. Conclusions

Process level simulations of aerosol-cirrus interactions allow to elucidate the intricate interplay between dynamical forcing and aerosol particle properties that ultimately determine cirrus properties at formation. We investigate the importance of mineral dust and aviation soot INPs in cirrus formation in distinct dynamical forcing regimes. Thereby, we account for variability in INP number concentrations and updraft speeds.

Generally, homogeneous freezing dominates in clear-sky aerosol-cirrus interactions above a threshold updraft speed determined by total number concentrations and ice nucleation ability of INPs. Given significant atmospheric variability in these INP properties as well as the presence of infrequent, yet large updraft speeds caused by mesoscale gravity waves, this strongly suggests that both, INP-induced ice nucleation and homogeneous freezing determine global cirrus properties.

Mineral dust reduces homogeneously nucleated ice crystal numbers much more strongly than aviation soot (61% vs. 12.5%) at a typically observed mean updraft speed of 15 cm s^{-1}. When dust and aviation soot are present in the same air mass, dust supersedes soot-cirrus interactions for dust particle number concentrations above 10 L^{-1} in most dynamical forcing situations.

Cirrus predominantly form on aviation soot only at updraft speeds below 5–10 cm s^{-1} and in dust-poor regions with dust particle number concentrations below 5 L^{-1}. Partial activation of aviation soot creates cirrus clouds whose properties are sensitive to mean size and size spread of the soot particle size distribution after contrail processing.

Pre-existing cloud ice suppresses aerosol-cirrus interactions at updrafts speeds below about 25 cm s^{-1} at ice crystal number concentrations of 10 L^{-1}, unless water vapor deposition coefficients are below 0.1.

We point out that the role of aviation soot in cirrus formation could even be smaller than estimated here due to the presence of INPs other than dust. Additional INP types include ammonium sulfate aerosol particles

(Abbatt et al., 2006), organic particles present in amorphous solid or semi-solid states (Murray et al., 2010), and biomass burning smoke particles that have been found to be widespread throughout the UT (Schill et al., 2020).

Liquid surface coatings present on INPs, not accounted for here, predominantly reduce their ice activity. Such a reduction in ice activity can be understood by blocking of pores in the PCF framework. More targeted research is needed to better understand how and on which timescales coatings affect ice nucleation in porous particles. With regard to aviation soot, future field studies should include concomitant measurements of size distribution and composition of ice crystal residuals sampled in fresh aircraft plumes and behind dissipating contrails. Finally, relating field observations to models will greatly benefit from measurements of vertical wind speed statistics during ice nucleation events.

Appendix A: Ice Activity of Mineral Dust and Aviation Soot

We make use of a number-based PSD, df/dD, for mineral dust particles (spherical-equivalent diameter D) from aircraft measurements (Froyd et al., 2022) (their Figure S10a). This PSD is an average over three individual PSDs outside of dust plumes, which by themselves show little variations at different n_d-levels, and is therefore representative of extratropical NH UT conditions. We calculate the ice activity per dust particle, $\mathcal{A}$, based on the parameterization provided by Ullrich et al. (2017). This laboratory study investigated desert dust samples that were collected from different locations around the world. We integrate the ice-active PSD, $\mathcal{A}df/dD$, as the fractional number concentration of dust particles in a given size range that form ice at a given ice supersaturation and temperature over all sizes (df/dD is normalized to unity, i.e., scaled by n_d), as described in K22.

Figure A1 shows the normalized average PSD from the *in-situ* measurements, the same PSD combined with the ice activity parameterization, and the resulting cumulative ice-active fraction used in the parameterization (K22). The dust PSD contains sub-micrometer and super-micrometer particles from the accumulation and coarse mode, respectively. At $T = 220$ K, the ice activity of dust increases most strongly for s-values in the range 0.35–0.4, the 50% activation level being reached at about $s = 0.375$. The ice-active PSD shows that at $s = 0.35$, only dust particles with $D > 1$ µm are ice-active. Once s attains values > 0.4, most of the smaller dust particles become ice-active, too.

Corresponding PSDs and ice activities of aviation soot are presented in Figure A2, covering the baseline case Soot as well as the cases with smaller and larger soot particles used in the sensitivity studies Soot-S and Soot-L. Ice-active PSDs drop off rapidly at mobility diameters of about 40 nm, because most soot aggregates are not significantly larger than the size of the constituent primary spherules, rendering soot PCF inefficient (K21). The key difference to dust is that size-integrated ice-active aviation soot fractions do not increase beyond 1% at homogeneous freezing levels ($s \geq 0.5$).

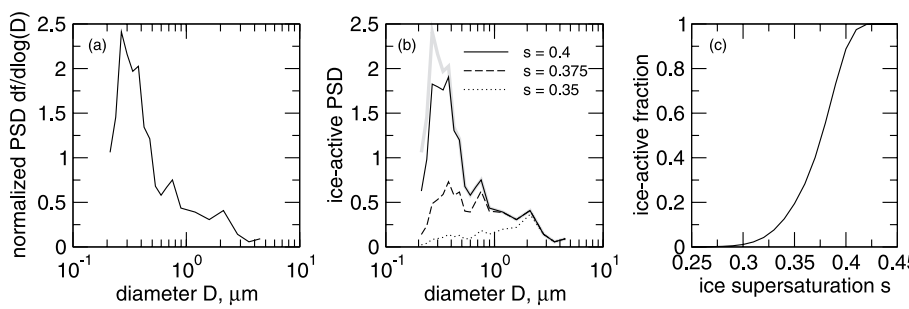

Figure A1. Dust particle number-size distribution normalized to unity (a), corresponding ice-active size spectrum at different values of ice supersaturation (b), and the associated size-integrated ice-active fraction (c). Panel (b) repeats the PSD from panel (a) as the heavy gray curve for ease of comparison.

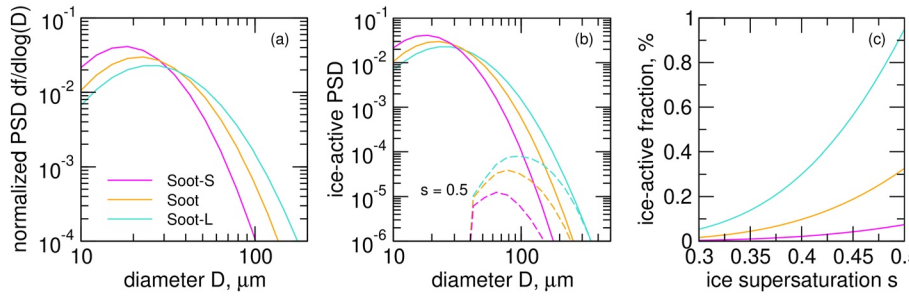

Figure A2. Similar to Figure A1, but for aviation soot particles. PSDs from the sensitivity studies Soot-S and Soot-L are also shown. PSDs from panel (a) are repeated in panel (b) as solid curves to directly compare with the corresponding ice-active PSDs (dashed).

Data Availability Statement

The data that support the findings of this study are publicly available (Kärcher, Marcolli, & Mahrt, 2022).

Acknowledgments
B.K. thanks Darrel Baumgardner for discussing airborne cirrus measurements. F.M. acknowledges funding from the European Union's Horizon 2020 research and innovation programme under the Marie Skłodowska-Curie Grant Agreement 890200 (MICROSCOPE project). Open Access funding enabled and organized by Projekt DEAL.

References

Abbatt, J. P. D., Benz, S., Cziczo, D. J., Kanji, Z., Lohmann, U., & Möhler, O. (2006). Solid ammonium sulfate aerosols as ice nuclei: A pathway for cirrus cloud formation. *Science*, *313*(5794), 1770–1773. https://doi.org/10.1126/science.1129726

Anderson, B. E., Cofer, W. R., Crawford, J., Gregory, G. L., Vay, S. A., Brunke, K. E., et al. (1999). An assessment of aircraft as a source of particles to the upper troposphere. *Geophysical Research Letters*, *26*(20), 3069–3072. https://doi.org/10.1029/1999GL900276

Baumgardner, D., Abel, S. J., Axisa, D., Cotton, R., Crosier, J., Field, P., et al. (2017). Cloud ice properties: In situ measurement challenges. *Meteorological Monographs*, *58*, 9.1–9.23. https://doi.org/10.1175/AMSMONOGRAPHS-D-16-0011.1

Bhandari, J., China, S., Chandrakar, K. K., Kinney, G., Cantrell, W., Shaw, R. A., et al. (2019). Extensive soot compaction by cloud processing from laboratory and field observations. *Scientific Reports*, *9*(1), 11824. https://doi.org/10.1038/s41598-019-48143-y

Bi, Y., Cao, B., & Li, T. (2017). Enhanced heterogeneous ice nucleation by special surface geometry. *Nature Communications*, *8*(1), 15372. https://doi.org/10.1038/ncomms15372

Bond, T. C., Doherty, S. J., Fahey, D. W., Forster, P. M., Berntsen, T., DeAngelo, B. J., et al. (2013). Bounding the role of black carbon in the climate system: A scientific assessment. *Journal of Geophysical Research*, *118*(11), 5380–5552. https://doi.org/10.1002/jgrd.50171

Brunner, C., Brem, B. T., Coen, M. C., Conen, F., Hervo, M., Henne, S., et al. (2021). The contribution of Saharan dust to the ice-nucleating particle concentrations at the High Altitude Station Jungfraujoch (3580 m a.s.l.), Switzerland. *Atmospheric Chemistry and Physics*, *21*(23), 18029–18053. https://doi.org/10.5194/acp-21-18029-2021

China, S., Kulkarni, G., Scarnato, B. V., Sharma, N., Pekour, M., Shilling, J. E., et al. (2015). Morphology of diesel soot residuals from supercooled water droplets and ice crystals: Implications for optical properties. *Environmental Research Letters*, *10*(11), 114010. https://doi.org/10.1088/1748-9326/10/11/114010

Cziczo, D. J., Froyd, K. D., Gallavardin, S. J., Möhler, O., Benz, S., Saathoff, H., & Murphy, D. M. (2009). Deactivation of ice nuclei due to atmospherically relevant surface coatings. *Environmental Research Letters*, *4*, 044013. https://doi.org/10.1088/1748-9326/4/4/044013

David, R. O., Marcolli, C., Fahrni, J., Qiu, Y., Sirkin, Y. A. P., Molinero, V., et al. (2019). Pore condensation and freezing is responsible for ice formation below water saturation for porous particles. *Proceedings of the National Academy of Sciences of the United States of America*, *116*(17), 8184–8189. https://doi.org/10.1073/pnas.1813647116

DeMott, P. J., Cziczo, D. J., Prenni, A. J., Murphy, D. M., Kreidenweis, S. M., Thomson, D. S., et al. (2003). Measurements of the concentration and composition of nuclei for cirrus formation. *Proceedings of the National Academy of Sciences of the United States of America*, *100*(25), 14655–14660. https://doi.org/10.1073/pnas.2532677100

Forster, P., Storelvmo, T., Armour, K., Collins, W., Dufresne, J.-L., Frame, D., et al. (2021). The Earth's energy budget, climate feedbacks, and climate sensitivity. *Climate Change 2021: The Physical Science Basis. Contribution of Working Group I to the Sixth Assessment Report of the Intergovernmental Panel on Climate Change*. Retrieved from www.ipcc.ch/report/ar6/wg1/downloads/report/IPCC_AR6_WGI_Chapter07.pdf

Froyd, K. D., Murphy, D. M., Brock, C. A., Campuzano-Jost, P., Dibb, J. E., Jimenez, J.-L., et al. (2019). A new method to quantify mineral dust and other aerosol species from aircraft platforms using single-particle mass spectrometry. *Atmospheric Measurement Techniques*, *12*(11), 6209–6239. https://doi.org/10.5194/amt-12-6209-2019

Froyd, K. D., Yu, P., Schill, G. P., Brock, C. A., Kupc, A., Williamson, C. J., et al. (2022). Dominant role of mineral dust in cirrus cloud formation revealed by global-scale measurements. *Nature Geoscience*, *15*(3), 177–183. https://doi.org/10.1038/s41561-022-00901-w

Gao, K., Friebel, F., Zhou, C.-W., & Kanji, Z. A. (2022). Enhanced soot particle ice nucleation ability induced by aggregate compaction and densification. *Atmospheric Chemistry and Physics*, *22*(7), 4985–5016. https://doi.org/10.5194/acp-22-4985-2022

Gao, K., & Kanji, Z. A. (2022a). Impacts of cloud-processing on ice nucleation of soot particles internally mixed with sulfate and organics. *Journal of Geophysical Research*, *127*(22). https://doi.org/10.1029/2022JD037146

Gao, K., & Kanji, Z. A. (2022b). Impacts of simulated contrail processing and organic content change on the ice nucleation of soot particles. *Geophysical Research Letters*, *49*(16). https://doi.org/10.1029/2022GL099869

Gettelman, A., & Chen, C. (2013). The climate impact of aviation aerosols. *Geophysical Research Letters*, *20*(11), 2785–2789. https://doi.org/10.1002/grl.5052

Harrington, J. Y., & Pokrifka, G. F. (2021). Approximate models for lateral growth on ice crystal surfaces during vapor depositional growth. *Journal of the Atmospheric Sciences*, *78*(3), 967–981. https://doi.org/10.1175/JAS-D-20-0228.1

Hong, Y., & Liu, G. (2015). The characteristics of ice cloud properties derived from CloudSat and CALIPSO measurements. *Journal of Climate*, *28*(9), 3880–3901. https://doi.org/10.1175/JCLI-D-14-00666.1

Hoyle, C. R., Luo, B. P., & Peter, T. (2005). The origin of high ice crystal number densities in cirrus clouds. *Journal of the Atmospheric Sciences*, *62*(7), 2568–2579. https://doi.org/10.1175/JAS3487.1

Jantsch, E., & Koop, T. (2021). Cloud activation via formation of water and ice on various types of porous aerosol particles. *ACS Earth Space Chem*, *5*(3), 604–617. https://doi.org/10.1021/acsearthspacechem.0c00330

Jensen, E. J., Lawson, R. P., Bergman, J. W., Pfister, L., Bui, T. V., & Schmitt, C. G. (2013). Physical processes controlling ice concentrations in synoptically forced, midlatitude cirrus. *Journal of Geophysical Research*, *118*(11), 5348–5360. https://doi.org/10.1002/jgrd.50421

Kanji, Z. A., Ladino, L. A., Wex, H., Boose, Y., Burkert-Kohn, M., Cziczo, D. J., & Krämer, M. (2017). Overview of ice nucleating particles. *Meteorological Monographs*, *58*, 1.1–1.33. https://doi.org/10.1175/AMSMONOGRAPHS-D-16-0006.1

Kärcher, B. (2022). A parameterization of cirrus cloud formation: Revisiting competing ice nucleation. *Journal of Geophysical Research*, *127*(18). https://doi.org/10.1029/2022JD036907

Kärcher, B., DeMott, P. J., Jensen, E. J., & Harrington, J. Y. (2022). Studies on the competition between homogeneous and heterogeneous ice nucleation in cirrus formation. *Journal of Geophysical Research*, *127*(3). https://doi.org/10.1029/2021JD035805

Kärcher, B., & Lohmann, U. (2002). A parameterization of cirrus cloud formation: Homogeneous freezing including effects of aerosol size. *Journal of Geophysical Research*, *107*(D23), AAC9-1–AAC9–10. https://doi.org/10.1029/2001JD001429

Kärcher, B., Mahrt, F., & Marcolli, C. (2021). Process-oriented analysis of aircraft soot-cirrus interactions constrains the climate impact of aviation. *Commun. Earth Environ.*, *2*(1), 113. https://doi.org/10.1038/s43247-021-00175-x

Kärcher, B., Marcolli, C., & Mahrt, F. (2022). The role of mineral dust aerosol particles in aviation soot-cirrus interactions [Dataset]. Zenodo. https://doi.org/10.5281/zenodo.7404707

Kärcher, B., Möhler, O., DeMott, P. J., Pechtl, S., & Yu, F. (2007). Insights into the role of soot aerosols in cirrus cloud formation. *Atmospheric Chemistry and Physics*, *7*(16), 4203–4227. https://doi.org/10.5194/acp-7-4203-2007

Kärcher, B., & Podglajen, A. (2019). A stochastic representation of temperature fluctuations induced by mesoscale gravity waves. *Journal of Geophysical Research*, *124*(21), 11506–11529. https://doi.org/10.1029/2019JD030680

Kaufmann, L., Marcolli, C., Hofer, J., Pinti, V., Hoyle, C. R., & Peter, T. (2016). Ice nucleation efficiency of natural dust samples in the immersion mode. *Atmospheric Chemistry and Physics*, *16*(17), 11177–11206. https://doi.org/10.5194/acp-16-11177-2016

Kay, J. E., & Wood, R. (2008). Timescale analysis of aerosol sensitivity during homogeneous freezing and implications for upper tropospheric water vapor budgets. *Geophysical Research Letters*, *35*(10). https://doi.org/10.1029/2007GL032628

Koehler, K. A., Kreidenweis, S. M., DeMott, P. J., Petters, M. D., Prenni, A. J., & Möhler, O. (2010). Laboratory investigations of the impact of mineral dust aerosol on cold cloud formation. *Atmospheric Chemistry and Physics*, *10*(23), 11955–11968. https://doi.org/10.5194/acp-10-11955-2010

Krämer, M., Rolf, C., Spelten, N., Afchine, A., Fahey, D., Jensen, E., et al. (2021). A microphysics guide to cirrus – Part 2: Climatologies of clouds and humidity from observations. *Atmospheric Chemistry and Physics*, *21*, 12569–12608. https://doi.org/10.5194/acp-20-12569-2020

Kreidenweis, S. M., Petters, M., & Lohmann, U. (2019). 100 years of progress in cloud physics, aerosols, and aerosol chemistry research. *Meteorological Monographs*, *59*, 11.1–11.72. https://doi.org/10.1175/AMSMONOGRAPHS-D-18-0024.1

Kuebbeler, M., Lohmann, U., Hendricks, J., & Kärcher, B. (2014). Dust ice nuclei effects on cirrus clouds. *Atmospheric Chemistry and Physics*, *14*(6), 3027–3046. https://doi.org/10.5194/acp-14-3027-2014

Lamb, D., & Verlinde, J. (2011). *Physics and Chemistry of clouds*. University Press.

Lee, D. S., Fahey, D. W., Skowron, A., Allen, M. R., Burkhardt, U., Chen, Q., et al. (2021). The contribution of global aviation to anthropogenic climate forcing for 2000 to 2018. *Atmospheric Environment*, *244*, 117834. https://doi.org/10.1016/j.atmosenv.2020.117834

Mahrt, F., Kilchhofer, K., Marcolli, C., Grönquist, P., David, R. O., Rösch, M., et al. (2020). The impact of cloud processing on the ice nucleation abilities of soot particles at cirrus temperatures. *Journal of Geophysical Research*, *125*(3). https://doi.org/10.1029/2019JD030922

Mahrt, F., Marcolli, C., David, R. O., Grönquist, P., Meier, E. J. B., Lohmann, U., & Kanji, Z. A. (2018). Ice nucleation abilities of soot particles determined with the Horizontal Ice Nucleation Chamber. *Atmospheric Chemistry and Physics*, *18*, 13363–13392. https://doi.org/10.5194/acp-18-13363-2018

Marcolli, C. (2014). Deposition nucleation viewed as homogeneous or immersion freezing in pores and cavities. *Atmospheric Chemistry and Physics*, *14*(4), 2071–2104. https://doi.org/10.5194/acp-14-2071-2014

Marcolli, C. (2017). Pre-activation of aerosol particles by ice preserved in pores. *Atmospheric Chemistry and Physics*, *17*(3), 1595–1622. https://doi.org/10.5194/acp-17-1595-2017

Marcolli, C. (2020). Technical note: Fundamental aspects of ice nucleation via pore condensation and freezing including Laplace pressure and growth into macroscopic ice. *Atmospheric Chemistry and Physics*, *20*(5), 3209–3230. https://doi.org/10.5194/acp-20-3209-2020

Marcolli, C., Mahrt, F., & Kärcher, B. (2021). Soot PCF: Pore condensation and freezing framework for soot aggregates. *Atmospheric Chemistry and Physics*, *21*. https://doi.org/10.5194/acp-2020-1134

McGraw, Z., Storelvmo, T., Samset, B. H., & Stjern, C. W. (2020). Global radiative impacts of black carbon acting as ice nucleating particles. *Geophysical Research Letters*, *47*(20). https://doi.org/10.1029/2020GL089056

Möhler, O., Benz, S., Saathoff, H., Schnaiter, M., Wagner, R., Schneider, J., et al. (2008). The effect of organic coating on the heterogeneous ice nucleation efficiency of mineral dust aerosols. *Environmental Research Letters*, *3*(2), 025007. https://doi.org/10.1088/1748-9326/3/2/025007

Moore, R. H., Thornhill, K. L., Weinzierl, B., Sauer, D., D'Ascoli, E., Kim, J., et al. (2017). Biofuel blending reduces particle emissions from aircraft engines at cruise conditions. *Nature*, *543*(7645), 411–415. https://doi.org/10.1038/nature21420

Mukherjee, S. (2013). *The science of clays*. Springer.

Murray, B. J., O'Sullivan, D., Atkinson, J. D., & Webb, M. E. (2012). Ice nucleation by particles immersed in supercooled cloud droplets. *Chemical Society Reviews*, *41*(19), 6519. https://doi.org/10.1039/c2cs35200a

Murray, B. J., Wilson, T. W., Dobbie, S., Cui, Z., Al-Jumur, S. M. R. K., Möhler, O., et al. (2010). Heterogeneous nucleation of ice particles on glassy aerosols under cirrus conditions. *Nature Geoscience*, *3*(4), 233–237. https://doi.org/10.1038/ngeo817

Nichman, L., Wolf, M., Davidovits, P., Onasch, T. B., Zhang, Y., Worsnop, D. R., et al. (2019). Laboratory study of the heterogeneous ice nucleation on black-carbon-containing aerosol. *Atmospheric Chemistry and Physics*, *19*, 12175–12194. https://doi.org/10.5194/acp-19-12175-2019

Penner, J. E., Zhou, C., Garnier, A., & Mitchell, D. L. (2018). Anthropogenic aerosol indirect effects in cirrus clouds. *Journal of Geophysical Research*, *123*(20). https://doi.org/10.1029/2018jd029204

Pitari, G., Iachetti, D., Genova, G. D., Luca, N. D., Sovde, O. A., Hodnebrog, O., et al. (2015). Impact of coupled NO_x/aerosol aircraft emissions on ozone photochemistry and radiative forcing. *Atmosphere*, *6*, 751–782. https://doi.org/10.3390/atmos6060751

Podglajen, A., Hertzog, A., Plougonven, R., & Legras, B. (2016). Lagrangian temperature and vertical velocity fluctuations due to gravity waves in the lower stratosphere. *Geophysical Research Letters*, *43*(7), 3543–3553. https://doi.org/10.1002/2016GL068148

Primm, K. M., Schill, G. P., Veghte, D. P., Freedman, M. A., & Tolbert, M. A. (2017). Depositional ice nucleation on NX illite and mixtures of NX illite with organic acids. *Journal of Atmospheric Chemistry*, *74*(1), 55–69. https://doi.org/10.1007/s10874-016-9340-x

Righi, M., Hendricks, J., & Beer, C. G. (2021). Exploring the uncertainties in the aviation soot-cirrus effect. *Atmospheric Chemistry and Physics*, *21*(23), 17267–17289. https://doi.org/10.5194/acp-21-17267-2021

Schill, G. P., Froyd, K. D., Bian, H., Kupc, A., Williamson, C., Brock, C. A., et al. (2020). Widespread biomass burning smoke throughout the remote troposphere. *Nature Geoscience*, *13*(6), 422–427. https://doi.org/10.1038/s41561-020-0586-1

Schoeberl, M. R., Jensen, E., Podglajen, A., Coy, L., Lodha, C., Candido, S., & Carver, R. (2017). Gravity wave spectra in the lower stratosphere diagnosed from project loon balloon trajectories. *Journal of Geophysical Research*, *122*(16), 8517–8524. https://doi.org/10.1002/2017JD026471

Schumann, U., Baumann, R., Baumgardner, D., Bedka, S. T., Duda, D. P., Freudenthaler, V., et al. (2017). Properties of individual contrails: A compilation of observations and some comparisons. *Atmospheric Chemistry and Physics*, *17*(1), 403–438. https://doi.org/10.5194/acp-17-403-2017

Shi, X., Liu, X., & Zhang, K. (2015). Effects of pre-existing ice crystals on cirrus clouds and comparison between different ice nucleation parameterizations with the Community Atmosphere Model (CAM5). *Atmospheric Chemistry and Physics*, *15*(3), 1503–1520. https://doi.org/10.5194/acp-15-1503-2015

Shi, Z., Zhang, D., Hayashi, M., Ogata, H., Ji, H., & Fujiie, W. (2008). Influences of sulfate and nitrate on the hygroscopic behaviour of coarse dust particles. *Atmospheric Environment*, *42*(4), 822–827. https://doi.org/10.1016/j.atmosenv.2007.10.037

Sullivan, R. C., Guazzotti, S. A., Sodeman, D. A., & Prather, K. A. (2007). Direct observations of the atmospheric processing of Asian mineral dust. *Atmospheric Chemistry and Physics*, *7*(5), 1213–1236. https://doi.org/10.5194/acp-7-1213-2007

Ullrich, R., Hoose, C., Möhler, O., Niemand, M., Wagner, R., Höhler, K., et al. (2017). A new ice nucleation active site parameterization for desert dust and soot. *Journal of the Atmospheric Sciences*, *74*(3), 699–717. https://doi.org/10.1175/JAS-D-16-0074.1

Wang, B., Knopf, D. A., China, S., Arey, B. W., Harder, T. H., Gilles, M. K., & Laskin, A. (2016). Direct observation of ice nucleation events on individual atmospheric particles. *Phys. Chem. Chem. Phys.*, *18*(43), 29721–29731. https://doi.org/10.1039/c6cp05253c

Welti, A., Lüönd, F., Stetzer, O., & Lohmann, U. (2009). Influence of particle size on the ice nucleating ability of mineral dusts. *Atmospheric Chemistry and Physics*, *9*(18), 6705–6715. https://doi.org/10.5194/acp-9-6705-2009

Wiacek, A., & Peter, T. (2009). On the availability of uncoated mineral dust ice nuclei in cold cloud regions. *Geophysical Research Letters*, *36*(17), L17801. https://doi.org/10.1029/2009GL039429

Zhang, C., & Harrington, J. Y. (2014). Including surface kinetic effects in simple models of ice vapor diffusion. *Journal of the Atmospheric Sciences*, *71*(1), 372–390. https://doi.org/10.1175/JAS-D-13-0103.1

Zhang, C., Zhang, Y., Wolf, M. J., Nichman, L., Shen, C., Onasch, T. B., et al. (2020). The effects of morphology, mobility size, and secondary organic aerosol (SOA) material coating on the ice nucleation activity of black carbon in the cirrus regime. *Atmospheric Chemistry and Physics*, *20*(22), 13957–13984. https://doi.org/10.5194/acp-20-13957-2020

Zhu, J., Penner, J. E., Garnier, A., Boucher, O., Gao, M., Song, L., et al. (2022). Decreased aviation leads to increased ice crystal number and a positive radiative effect in cirrus clouds. *AGU Advances*, *3*(2). https://doi.org/10.1029/2021AV000546